NASA-TM-85412 19830025580

A Reproduced Copy

OF

NASA TM-85412

Reproduced for NASA

by the

NASA Scientific and Technical Information Facility

FFNo 672 Aug 65

ICASE

SPECTRAL MULTIGRID METHODS WITH APPLICATIONS

TO TRANSONIC POTENTIAL FLOW

Craig L. Streett
Thomas A. Zang
M. Yousuff Hussaini

Report No. 83-11

April 29, 1983

INSTITUTE FOR COMPUTER APPLICATIONS IN SCIENCE AND ENGINEERING
NASA Langley Research Center, Hampton, Virginia 23665

Operated by the

UNIVERSITIES SPACE USRA RESEARCH ASSOCIATION

SPECTRAL MULTIGRID METHODS WITH APPLICATIONS TO TRANSONIC POTENTIAL FLOW

Craig L. Streett
NASA Langley Research Center

Thomas A. Zang*
College of William and Mary

M. Yousuff Hussaini**
Institute for Computer Applications in Science and Engineering

Abstract

Spectral multigrid methods are demonstrated to be a competitive technique for solving the transonic potential flow equation. The spectral discretization, the relaxation scheme, and the multigrid techniques are described in detail. Significant departures from current approaches are first illustrated on several linear problems. The principal applications and examples, however, are for compressible potential flow. These examples include the relatively challenging case of supercritical flow over a lifting airfoil.

---

*Supported under NASA Contract No. NAG1-109.

**Supported under NASA Contract Nos. NAS1-17130 and NAS1-17070 while in residence at ICASE, NASA Langley Research Center, Hampton, VA 23665.

I. Introduction

Interest in transonic aerodynamics endures because most commercial and military aircraft operate predominantly in the transonic regime. The design and analysis of transonic wings and related configurations have been carried out largely within the framework of the transonic small perturbation equation and the full potential equation. Apart from their relative simplicity the popularity of these flow models is due to their adequate representation of flow features of practical importance. For instance, the pressure rise across an isentropic shock in these models is sufficiently accurate for normal Mach numbers ahead of the shock less than 1.3. Naturally, if other design considerations produce strong shocks and/or complex vortical flow, then recourse to the Euler equations is appropriate. Indeed, Euler solutions to transonic flow problems have attracted serious attention as of late, and they will surely gain increasing popularity as they become more competitive with potential solutions. However, for many configurations of engineering interest, potential flow predictions with asymptotically first-order weak viscous-inviscid interaction give solutions of more than adequate accuracy [1]. When strong shocks and/or vorticity are of dominant importance in the flow field, weak viscous-inviscid interaction is no longer an adequate model. Implementation of strong interaction models is relatively crude at this time, and until substantial improvements have been made, the potential formulation will retain the most favorable accuracy-to-cost ratio for a wide range of practical transonic flow problems.

The main difficulty in the numerical solution of the steady transonic flow problem has been the mixed elliptic-hyperbolic nature allowing for the presence of discontinuities. The initial breakthrough in overcoming this difficulty was made only in the early 1970's by Murman and Cole [2] who

introduced a type-dependent difference scheme for solving the transonic small perturbation equation. Following this breakthrough there have been many developments in the computation of transonic flows. The survey lectures of Ballhaus [3] and Jameson [4] present a detailed review of these developments up to 1976. Since then most research on numerical methods for the steady-state full potential equation has focused on accelerating iterative methods. Much of the progress has been made by relating the relaxation scheme to a time-dependent differential equation and then using the theory of numerical integration of ordinary or partial differential equations to estimate the optimal relaxation parameters. Ballhaus, et al. [5] developed approximate factorization schemes, AF1 and AF2, which, applied to the transonic small perturbation equation, yielded rapid convergence. The AF1 scheme is analogous to the Douglas-Gunn alternate direction implicit (ADI) method for the parabolic equation. The AF2 scheme, which is similarly related to a hyperbolic equation, has been extended by Holst to the full potential equation in conservation form [6] and to three dimensions [7]. Another variant of AF2 is the approximate factorization scheme AF3 developed by Baker [8] (independently of Holst) for the full potential equation in the nonconservative form. The success of all these schemes over the practical range of transonic flow conditions is still problem-dependent. Catherall [9] discusses the basic principle of the approximate factorization schemes for the two-dimensional steady potential equation, and describes a procedure for constructing optimal algorithms. Wong and Hafez [10] propose a preconditioned conjugate gradient method which is at least twice as fast as pure successive-line overrelaxation (SLOR). Some other iterative schemes are assessed by Doria and South [11]. Another fast method is the multigrid technique, first applied by South and Brandt [12] to the transonic small perturbation equation

with SLOR as a basic iterative scheme. Recently, Jameson [13] developed the multigrid procedure to accelerate convergence of the full potential solution by an ADI method. Despite the existence of quite a few efficient methods of potential solution, controlled comparisons are lacking.

The computer time required to obtain numerical solutions for two-dimensional potential flows is now so small that there is practically no incentive for developing more efficient schemes. However, for three-dimensional flows existing methods are still so costly that a substantially more efficient solution algorithm would have great practical importance. Unlike the two-dimensional case, computer storage is a crucial consideration in weighing the efficiency of a scheme. Pseudospectral methods have demonstrated their capacity for producing equivalent accuracy with far fewer grid points than standard second-order or even fourth-order methods, not only for smooth flows but also, more recently, for the Euler equations [14]. The first pseudospectral two-dimensional potential flow solutions were obtained by Streett [15], who established that equivalent solutions were in fact obtained for potential flows with far fewer grid points than required by standard methods. However, his solution technique was clearly in need of acceleration, particularly for supercritical flows. In this paper we describe an acceleration technique, based on the spectral multigrid methods developed by Zang, et al. [16], [17], that has significantly improved the rate of convergence of the pseudospectral discretization of the full potential equation. In fact, the spectral multigrid scheme is so efficient that the preliminary version described here is highly competitive with the finite difference schemes.

Since the application of spectral methods to compressible flows is still a fairly novel approach, most readers are likely to be unfamiliar with either

the practical details of spectral methods or the nuances of numerical methods for compressible flows. Moreover, spectral multigrid methods themselves are still in the formative stage. The promising nature of the present results warrants a reasonably complete and self-contained description of the numerical method.

We begin by describing a means of implementing pseudospectral differentiation, which, although asymptotically inefficient, is nonetheless preferable for problems on moderately-sized grids. This is followed by descriptions of the essential features of spectral multigrid methods and of the relaxation schemes. These methods are then illustrated on several linear problems. An explanation of the potential flow problem and its pseudospectral approximation is given next. Finally we report on the performance of the spectral multigrid method on both subcritical and supercritical potential flows.

II. Spectral Methods Using Matrix Multiples

The Fast Fourier Transform (FFT) has usually been cited as a key element in the efficiency and hence the implementation of spectral methods. In the pseudospectral sort of calculations discrete Fourier methods are commonly used in the evaluation of derivatives. However, under some circumstances it is actually faster to use conventional matrix-vector multiplications for this purpose than to resort to transform techniques. An obvious requirement is that the problem be of moderate size. There are many significant engineering applications which meet this requirement. The transonic flow application, which is the main thrust of this paper, is one such example. Even in circumstances which most favor transform techniques -- on grids with 2^k points -- the matrix-multiply approach (using nothing but Fortran) has proven

to be significantly faster than the transform method (employing assembly language FFT's). Precise comparisons will be given below.

In a pseudospectral method the fundamental representation of the solution is in physical space. The quantities which are stored are the values of the function $u(x)$ at special collocation points x_j. Derivatives, however, are evaluated spectrally. The values of the function are passed through a suitable discrete transform to produce the representation of the function in transform (wavenumber) space. The actual differentiation takes place in wavenumber space. Then an inverse transform is applied to yield the pseudospectral approximation to the derivatives of the function at the collocation points. Let U denote the vector of values of the function at the collocation points. Then the approximation to the derivative at these points may be written

$$O\,U, \tag{1}$$

where

$$O = C^{-1}\,D\,C, \tag{2}$$

with C representing the discrete transform and D representing differentiation in wavenumber space.

The most well-known pseudospectral method is based upon Fourier series. Let the interval of interest be $[0,2\pi]$ and use the collocation points

$$x_j = \frac{2\pi j}{M} \qquad j = 0,1,\cdots,M-1. \tag{3}$$

Then

$$C_{kj} = \frac{1}{M} e^{-\frac{2\pi i k j}{M}} \qquad \begin{matrix} k = -\frac{M}{2},\cdots,\frac{M}{2}-1 \\ j = 0,1,\cdots,M-1 \end{matrix} \tag{4}$$

$$D_{k\ell} = \begin{cases} ik\,\delta_{k,\ell} & k = -\frac{M}{2}+1,\cdots,\frac{M}{2}-1 \\ & \ell = -\frac{M}{2},\cdots,\frac{M}{2}-1 \\ 0 & k = -\frac{M}{2} \\ & \ell = -\frac{M}{2},\cdots,\frac{M}{2}-1 \end{cases} \tag{5}$$

$$(C^{-1})_{jk} = e^{\frac{2\pi ikj}{M}} . \tag{6}$$

The Fourier series differentiation matrix may be constructed by the matrix multiplies implied by Eq. (2). Alternatively, one may simply use the explicit formula given in Eqs. (8) and (9) of [16] for the elements of D.

Once the matrix D has been constructed, the cost of evaluating a derivative by the matrix vector product DU is $O(M^2)$. The transform technique reduces this to $O(M \ln M)$. However, two transforms are required and the constant in the $O(M \ln M)$ factor is larger than the one in the $O(M^2)$ case.

Chebyshev pseudospectral methods have been the most widely used ones for non-periodic boundary conditions. The standard interval is $[-1,1]$ and the collocation points are

$$x_j = \cos\frac{\pi j}{N} \qquad j = 0,1,\cdots,N. \tag{7}$$

Then

$$C_{kj} = \frac{2}{N\bar{c}_k\bar{c}_j}\cos\frac{\pi jk}{N} \qquad k,j = 0,1,\cdots,N\ , \tag{8}$$

where

$$\bar{c}_j = \begin{cases} 2 & j = 0 \text{ or } N \\ 1 & \text{otherwise} \end{cases} . \tag{9}$$

Moreover,

$$D_{k\ell} = \begin{cases} \frac{2\ell}{\bar{c}_k} & \ell > k+1 \quad \text{and} \quad \ell \equiv k+1 \pmod 2 \\ 0 & \text{otherwise} \end{cases} , \tag{10}$$

where

$$c_j = \begin{cases} 2 & j = 0 \\ 1 & \text{otherwise} \end{cases} \tag{11}$$

and

$$(C^{-1})_{jk} = \cos \frac{\pi jk}{N} . \tag{12}$$

An explicit formula is available in Eqs. (49) and (50) of [16] for this Chebyshev differentiation matrix.

III. Spectral Multigrid Fundamentals

Overview of Multigrid Algorithms

The problems of interest here are scalar partial differential boundary value problems. The PDE can be written in the general form

$$L(u) = f, \tag{13}$$

where $u(x,y)$ is the unknown function, $f(x,y)$ is some source term, and L is a partial differential operator which might be nonlinear in the unknown u. The corresponding discrete problem will be written

$$L(U) = F \tag{14}$$

in obvious notation.

Multigrid solution schemes for Eq. (14) involve combining relaxation sweeps for that equation with relaxation sweeps for related problems on coarser grids. Let V denote an approximation to U. The essential property for the relaxation scheme is that it preferentially damp the high-frequency components of the error $V - U$. Then after a small number of relaxations the error will have so little high-frequency content that it can be approximated well on a coarser grid. Solutions on the coarser grid are relatively inexpensive to obtain, especially if this strategy is applied recursively by using still coarser grids as needed.

Let us consider just the interplay between two grids. The fine-grid problem is written

$$L^f(U^f) = F^f. \tag{15}$$

The shift to the coarse grid occurs after the fine-grid approximation V^f has been sufficiently smoothed by the relaxation process, i.e., after the high-frequency content of the error $V^f - U^f$ has been sufficiently reduced. The related coarse-grid problem is

$$L^c(U^c) = F^c, \tag{16}$$

where

$$F^c = R[F^f - L^f(V^f)] + L^c(RV^f). \tag{17}$$

The restriction operator R interpolates a function from the fine grid to the coarse grid. The coarse-grid operator and solution are denoted by L^c and U^c, respectively. After an adequate approximation V^c to the coarse-grid

problem has been obtained, the fine-grid approximation is corrected via

$$V^f \leftarrow V^f + P(V^c - RV^f). \tag{18}$$

The prolongation operator P interpolates a function from the coarse grid to the fine grid.

The choice of the coarse-grid problem is based upon rewriting Eq. (15) as

$$L^f(U^f) = [F^f - L^f(V^f)] + L^f(V^f). \tag{19}$$

The term in brackets is the fine-grid residual. Since it has been presumed to be smooth, its coarse-grid approximation is clearly

$$R[F^f - L^f(V^f)]. \tag{20}$$

Equations (16) and (17) then follow by replacing the remaining fine-grid quantities with appropriate coarse-grid ones.

The quantity

$$W^c = U^c - RV^f \tag{21}$$

is the coarse-grid correction. Equations (16) to (18) are equivalent to

$$L^c(RV^f + W^c) - L^c(RV^f) = F^c \tag{22}$$

$$V^f \leftarrow V^f + PZ^c, \tag{23}$$

where Z^c is the approximation to W^c. For linear problems Eq. (22) reduces

to

$$L^c W^c = F^c. \tag{24}$$

This overview has, of course, been based upon the paper by Brandt [18], albeit in notation popularized by Hackbusch [19]. The particular choices of the interpolation and coarse-grid operators used in the present spectral multigrid work are described in the following sub-sections. This description is given for one-dimensional problems. The extension to higher dimensions is obvious. These details are followed by a discussion of the relaxation schemes.

Interpolation Operators

The spectral multigrid interpolation operators which were proposed in [16] for periodic coordinates amount to trigonometric interpolation: given a function on a coarse grid (with M_c points), compute the discrete Fourier coefficients and then use the resulting discrete Fourier series to construct the interpolated function on the fine grid (with M_f points). This may be accomplished by performing two FFT's. An explicit representation of the prolongation operator is

$$P_{jk} = \frac{1}{M_c} \sum_{\ell = -\frac{M_c}{2} + 1}^{\frac{M_c}{2} - 1} e^{2\pi i \ell \left(\frac{j}{M_f} - \frac{k}{M_c}\right)}, \tag{25}$$

which sums to yield

$$P_{jk} = \frac{1}{M_c} S\left(\frac{j}{M_f} - \frac{k}{M_c}\right), \tag{26}$$

where

$$S(r) = \begin{cases} N_c & r \text{ integer} \\ \sin(\pi r N_c)\cot(\pi r) - \cos(\pi r N_c) & \text{otherwise} \end{cases} . \qquad (27)$$

The corresponding restriction operator is essentially the adjoint of this:

$$R_{jk} = \frac{1}{N_f} S\left(\frac{j}{N_c} - \frac{k}{N_f}\right). \qquad (28)$$

Interpolation for non-periodic coordinates employs Chebyshev series in an analogous fashion. The prolongation operator is

$$P_{jk} = \frac{2}{\bar{c}_k N_c} \sum_{\ell=0}^{N_c}{}'' \bar{c}_\ell^{-1} \cos\frac{\pi \ell j}{N_f} \cos\frac{\pi \ell k}{N_c} , \qquad (29)$$

where $\bar{c}_k$ is defined by Eq. (9) with $N = N_c$. This sums to

$$P_{jk} = \frac{2}{\bar{c}_k N_c}\left[Q\left(\frac{j}{N_f} - \frac{k}{N_c}\right) + Q\left(\frac{j}{N_f} + \frac{k}{N_c}\right)\right], \qquad (30)$$

where

$$Q(r) = \begin{cases} \frac{N_c}{2} & r \text{ integer} \\ \frac{1}{4} - \frac{1}{4}\cos(\pi r N_c) + \frac{1}{2}\cos\left(\frac{\pi r}{2}(N_c+1)\right)\sin\left(\frac{\pi r N_c}{2}\right)\csc\left(\frac{\pi r}{2}\right) & \text{otherwise} \end{cases} . \qquad (31)$$

We will have occasion to use two distinct restriction operators. One is sometimes used in forming the coarse-grid operator and is obtained by applying Chebyshev restriction in the obvious fashion. It will be denoted by $R^{(o)}$ and it is given by

$$R^{(o)}_{jk} = \frac{2}{\bar{c}_k N_f}\left[\bar{Q}\left(\frac{j}{N_c} - \frac{k}{N_f}\right) + \bar{Q}\left(\frac{j}{N_c} + \frac{k}{N_f}\right)\right], \qquad (32)$$

where $\bar{c}_k$ is defined by Eq. (9) with $N = N_f$ and

$$\bar{Q}(r) = \begin{cases} 1/4 + \frac{N_c}{2} & r \text{ integer} \\ 1/4 + 1/2 \cos\left(\frac{\pi r}{2}(N_c+1)\right)\sin\left(\frac{\pi r N_c}{2}\right)\csc\left(\frac{\pi r}{2}\right) & \text{otherwise} \end{cases} . \quad (33)$$

The other is used for interpolation, is denoted by $R^{(i)}$, and is defined by the adjoint requirement:

$$R^{(i)}_{jk} = \frac{2}{\bar{c}_k N_c}\left[Q\left(\frac{j}{N_c} - \frac{k}{N_f}\right) + Q\left(\frac{j}{N_c} + \frac{k}{N_f}\right)\right], \quad (34)$$

where $\bar{c}_k$ is defined by Eq. (9) with $N = N_c$.

Coarse-Grid Operator

A typical term in the class of problems considered here is

$$\frac{d}{dx}\left[a(u,x)\,\frac{du}{dx}\right]. \quad (35)$$

The discrete operator which represents its fine-grid pseudospectral approximation is

$$L^f = O\,A\,O, \quad (36)$$

where O is given by Eq. (2) and A is the diagonal matrix

$$A_{jk} = a(u_j, x_j)\delta_{j,k}. \quad (37)$$

Many multigrid investigators, e.g., [19], [20], and [21], have advocated choosing the coarse-grid operator so that

$$L^c = RL^fP. \tag{38}$$

Both the Fourier and the Chebyshev first-derivative operators, defined by Eqs. (2) - (12), satisfy

$$O^c = RO^fP, \tag{39}$$

where $R = R^{(o)}$ is chosen in the Chebyshev case. However, Eq. (38) itself is not satisfied if the coarse-grid analog of Eq. (36) is used to define L^c, except in the trivial case for which $a(u,x)$ is a constant. On the other hand, much of the efficiency of the pseudospectral method is lost if Eq. (38) is used to define the coarse-grid operator. Some compromises were suggested in [17]. The most satisfactory one seems to be using Eq. (36) but with the restricted values of $a(u_j,x_j)$ in place of the pointwise values. The Chebyshev restrictions should be performed with $R^{(o)}$.

Boundary Conditions

In the applications that follow, three types of boundary conditions appear: periodic, Dirichlet, and Neumann. Periodic boundary conditions are automatically satisfied by the use of Fourier series. Fully-periodic problems contain some subtleties that are discussed in [17].

Dirichlet boundary conditions are handled effortlessly. The vector of unknowns should include the values at the boundary points in their natural locations. (This has the side effect of facilitating the programming of the Chebyshev interpolation.) On the fine grid the desired boundary values are

inserted into the appropriate locations and these values are not modified during the relaxation. On the coarser grids the appropriate boundary values are the ones which fall out of the restriction process.

Neumann boundary conditions are a bit touchier. We have enforced them by incorporating the Neumann boundary condition into the discrete operator. Suppose that there is a Neumann boundary condition at $x = -1$. In the evaluation of a term such as appears in Eq. (35), the first stage is the computation of du/dx at all the collocation points. In general this value will not match the desired boundary value. The boundary condition is enforced by resetting the value of du/dx at $x = -1$ to the desired value before proceeding with the multiplication by $a(u,x)$ and then the final differentiation. This produces the desired boundary condition in the converged solution. This approach has the advantage of ensuring that the boundary condition appears in the discrete operator with a consistent scaling. A much less effective alternative is to replace the differential equation at $x = -1$ with the condition that du/dx is the prescribed boundary value. The disadvantage of this approach is that this boundary equation is far out of scale with the rest of the operator. This alternative has in fact been tried on some of our test problems and it has resulted in a substantial deterioration of the convergence rate.

IV. Relaxation Schemes

The crucial property that a relaxation scheme should possess for use in a multigrid algorithm is that it damp effectively the high-frequency components of the error. It need not be especially effective in the low-frequency range, so long as it does not amplify any components. For spectral multigrid methods

an additional requirement arises from the global nature of the approximation: the fast evaluation of derivatives demands that the relaxation be simultaneous rather than successive, e.g., Jacobi's method can be implemented efficiently, whereas Gauss-Seidel's cannot.

A class of iterative schemes that meets these requirements is based upon approximate factorization techniques [5]. These methods are especially attractive because they have been employed in some of the most successful finite difference solutions to the delicate transonic potential flow problem [7], [13]. Moreover, the latter work demonstrated their effectiveness in the multigrid context, albeit for a purely finite difference approximation. A review of the computational transonics literature suggests that the most fruitful interpretation of approximate factorization schemes for this mixed elliptic-hyperbolic problem is in terms of their corresponding time-dependent partial differential equation. This is the approach that will be taken below.

An alternative and perhaps more traditional interpretation for linear, elliptic problems is in terms of preconditioning. The relaxation scheme proposed in [17] for a spectral multigrid method for such problems was interpreted as an incomplete LU decomposition serving as a preconditioning for Richardson's iteration. A brief description of this scheme is included here since it will serve as a comparison for the approximate factorization method on one of the linear test problems.

Richardson Iteration with Incomplete LU Decomposition

A preconditioned Richardson iteration for solving Eq. (14) can be expressed as

$$V \leftarrow V + \omega H^{-1}[F - L(V)], \tag{40}$$

where H is the preconditioning matrix and ω is the relaxation parameter. The matrix H should be chosen so that it is an approximate inverse to L, but is easily invertible. The version recommended in [17] for linear problems is obtained by first constructing the matrix H_{FD} which represents a standard second-order finite difference approximation to $\mathcal{L}$ (see Eq. (13)) and then performing an incomplete LU decomposition of H_{FD}. Details are provided in [17] along with a prescription for choosing the relaxation parameter ω so that the high-frequency error components are damped preferentially.

Approximate Factorization

For this discussion it is convenient to rewrite Eq. (14) as

$$M(U) = 0, \tag{41}$$

where of course,

$$M(U) = L(U) - F. \tag{42}$$

Next, view U not as the solution to Eq. (41), but rather as the steady-state solution to the evolution equation

$$\frac{\partial U}{\partial t} = M(U). \tag{43}$$

This is surely sensible if $\mathcal{L}(u)$ is elliptic for then Eq. (43) represents the spatial discretization of a parabolic problem. Semi-implicit time-stepping procedures are desirable for such problems because of the severe explicit time-step limitations. (This is especially acute for pseudospectral discretizations employing Chebyshev series because of the very small spacing between the collocation points near the boundary.) The simplest practical

time discretization of Eq. (43) is

$$\frac{U^{(n+1)} - U^{(n)}}{\Delta t} = M(U^{(n)}) + J(U^{(n)})(U^{(n+1)} - U^{(n)}), \tag{44}$$

where

$$J(U) = \frac{\partial M}{\partial U}(U), \tag{45}$$

and a superscript refers to a time level. Let

$$\alpha = \frac{1}{\Delta t} \tag{46}$$

and

$$\Delta U^{(n)} = U^{(n+1)} - U^{(n)}, \tag{47}$$

and then rewrite Eq. (44) as

$$[\alpha I - J(U^{(n)})]\Delta U^{(n)} = M(U^{(n)}), \tag{48}$$

where I denotes the identity matrix.

This motivates the relaxation scheme

$$V \leftarrow V + \omega \Delta V, \tag{49}$$

where ΔV is the solution to

$$[\alpha I - J(V)]\Delta V = M(V). \tag{50}$$

In many cases the Jacobian $J(V)$ can be split into the sum of two operators $J_x(V)$ and $J_y(V)$, each involving derivatives in only the one coordinate

direction indicated by the subscript. Approximate factorization methods encompass various approximations to the left-hand side of Eq. (48). The most straightforward of these is

$$[\alpha I - J_x(V)]\,[\alpha I - J_y(V)]\Delta V = \alpha M(V), \tag{51}$$

in combination with Eq. (49). This is just the Douglas-Gunn version of ADI [22]. It is commonly referred to as AF1 for the transonic problem [5]. For second-order spatial discretizations the term $[\alpha I - J_x(V)]$ leads to a set of tridiagonal systems, one for each value of y. The second left-hand side factor produces another set of tridiagonal systems. For pseudospectral discretizations, however, these systems are full; hence, Eq. (51) is still relatively expensive to invert. A compromise analogous to the one invoked in the incomplete LU decomposition preconditioning is to replace J_x and J_y with their second-order finite difference analogs, denoted by H_x and H_y, respectively:

$$[\alpha I - H_x(V)]\,[\alpha I - H_y(V)]\Delta V = \alpha M(V). \tag{52}$$

The approximate factorization scheme consists of Eqs. (49) and (52). For purely finite difference approximations some analytical results are available for selecting optimal values for the parameters α and ω [9]. No similar results are yet available for the present application. By analogy with the finite difference case we have chosen ω to be of order unity and have selected a sequence of α's in a range $[\alpha_\ell, \alpha_h]$ by the rule

$$\alpha^k = \alpha_h \left(\frac{\alpha_\ell}{\alpha_h}\right)^{\frac{k-1}{K-1}}, \tag{53}$$

where K denotes the number of distinct α's. The choices of α_ℓ and α_h were based in part on estimates of the eigenvalue range of the discrete operators and in (much greater) part by trial and error. Fortunately, the AF1 scheme is not very sensitive to these parameters.

For single-grid solutions to the subcritical potential flow problem the pseudospectral AF1 scheme based on Eq. (43) has proven satisfactory [15]. Extensive work on finite difference methods for supercritical potential flow has indicated the necessity to base their approximate factorization schemes on

$$\frac{\partial^2 U}{\partial s \partial t} = M(U), \tag{54}$$

where s is a physical variable directed along the streamline. One scheme which models this behavior is referred to as AF2 [5]. A pseudospectral AF2 variant is described in [15]. Since schemes of the AF2 type model hyperbolic equations they are relatively ineffective at damping high-frequency error components. Indeed, in the pseudospectral single-grid implementations [15] for supercritical flow, an iterative strategy involving both AF2 and AF1 was found to be more effective than AF2 alone. (By itself, of course, AF1 was divergent.) This will be referred to below as the AF2/AF1 scheme.

V. Numerical Results for Linear Problems

We chose a series of test problems to bridge the gap between the spectral multigrid methods described in [17] and those required for the potential flow problem. The first step was to change the relaxation scheme from preconditioned Richardson iteration to approximate factorization. The boundary conditions were left as Dirichlet in both coordinate directions. The

next phase involved shifting to periodic boundary conditions in one direction. In the final stage the geometry was altered from a rectangle to an annulus with an inner radial boundary condition of Neumann rather than Dirichlet type. This last problem is about as close as one can come to the potential flow problem within the constraint of linearity.

The multigrid codes used a maximum of 4 levels. These are labelled by the index k, where $k = 2, 3, 4,$ or 5. The grid on level k contains either 2^k (Fourier) or $2^k + 1$ (Chebyshev) collocation points in a coordinate direction (including boundary points). Two different schedules were used; they were referred to as schedules B and D in [17]. For schedule B the problem was first solved on level 2; then that solution was interpolated to level 3 as the initial guess for a multigrid iteration involving levels 2 and 3; then the converged level 3 solution was interpolated to level 4 as its initial guess, and so on until level 5. For schedule D the multigrid process simply began on level 5. In both cases the initial guess consisted of random numbers chosen from (0,1), ensuring that all error components were present initially. Both schedules were run in a fixed mode with 6 relaxations (2 passes through a 3 parameter sequence) before restriction to a coarser grid. A coarse-grid solution was deemed acceptable for prolongation to a fine-grid whenever its RMS residual dropped below 0.1% of the last residual on the finer grid. All of these linear runs employed the correction scheme, i.e., Eq. (24) rather than Eq. (16) was solved on the coarser levels. The variable coefficients and the right-hand sides for the coarse-grid problems were filtered in the manner described in [17].

The specific measure used was the equivalent smoothing rate. In some preliminary calculations the average time τ_0 required for a single fine-grid relaxation was determined. For an actual multigrid calculation let r_1 and

r_2 be the RMS residuals after the first and last fine-grid relaxations, respectively and let τ be the total CPU time. Then the equivalent smoothing rate was taken as

$$\left[\frac{r_2}{r_1}\right]^{\frac{1}{\frac{\tau}{\tau_0}-1}}. \tag{55}$$

Rectangular Chebyshev - Chebyshev Problem

The problem class is the same one examined in [17]:

$$\frac{\partial}{\partial x}\left[a\,\frac{\partial u}{\partial x}\right] + \frac{\partial}{\partial y}\left[a\,\frac{\partial u}{\partial y}\right] = f, \tag{56}$$

on $(-1,1) \times (-1,1)$ with Dirichlet boundary conditions with

$$a(x,y) = 1 + \varepsilon\, e^{\cos m_a \pi(x+y)}, \tag{57}$$

and $f(x,y)$ and the boundary data chosen so that the solution is

$$u(x,y) = \sin(m_u \pi x + \pi/4)\, \sin(m_u \pi y + \pi/4). \tag{58}$$

The properties of three test cases are listed in Table I. The parameters used in the approximate factorization scheme are given in Table II.

The performance of the preconditioned Richardson (PR) and the approximate factorization (AF) methods is shown in Table III. The PR method is about twice as fast as AF on these problems. But recall that the PR scheme has been highly tuned (especially for problem 1), whereas the AF scheme was subjected

to only a small amount of trial and error tuning. No doubt the AF scheme would benefit greatly from more experimentation, not to mention analysis. We have been content with establishing its workability in this multigrid context.

When derivative evaluations are performed via FFT's, the time required on a CDC Cyber-175 for a single level 5 relaxation (including both the residual evaluation and factorization stages) is 0.248 sec. for PR and 0.238 sec. for AF. Only about 5% of the total time in these calculations was spent interpolating between levels. On average there were 4 to 5 relaxations for every interpolation. A comparison between the transform and matrix-multiply methods of differentiation is provided in Table IV. Only on level 5 (a 33 × 33 grid) does one gain by using FFT's. Furthermore, since most of the work takes place on levels 2 to 4, the total running time is less (by 10 - 20%) for the matrix-multiply versions. Bear in mind that assembly language FFT's were performed on grids ideal for the FFT (powers of 2). The matrix multiplies were coded in Fortran. In the potential flow application it is advantageous to work on more general grids. Thus the matrix-multiply alternative is highly competitive. Its advantage ought to extend to even larger grids on vector processors.

Table I. Characteristics of the Rectangular Chebyshev-Chebyshev Test Problems

Problem No.	ε	m_u	m_a
1	0.00	1	1
2	0.20	2	2
3	1.00	5	5

Table II. Parameters of the AF Scheme for the Rectangular Chebyshev-Chebyshev Problems

Level	α_ℓ	α_h	ω
2	1	6	1.4
3	8	75	1.2
4	80	1000	1.1
5	600	8000	1.0

Table III. Equivalent Smoothing Rates on the Rectangular Chebyshev-Chebyshev Problems

Problem No.	PR	AF
1	.26	.43
2	.58	.78
3	.78	.92

Table IV. Residual Evaluation Time for the AF Scheme on the Rectangular Chebyshev-Chebyshev Test Problems

Level	Transform Method Differentiation	Matrix-Multiply Differentiation
3	.0204	.0083
4	.0622	.0390
5	.214	.248

Rectangular Chebyshev-Fourier Problem

This problem is also described by Eq. (56), but on $(-1,1) \times (0,2\pi)$ and with Dirichlet boundary conditions in x and periodicity in y. The coefficient

$$a(x,y) = 1 + \varepsilon\, e^{\cos m_a(\pi x+y)} \tag{59}$$

and the rest of the problem fits the solution

$$u(x,y) = \sin(m_u \pi x + \pi/4)\, \sin(m_u \pi \cos y + \pi/4). \tag{60}$$

The properties of three test cases are listed in Table V and the AF parameters are supplied in Table VI.

Table VII gives the results. There is evidently nothing to be gained here by working up to the finest level by first solving the coarser level problems. The present combination of the coarse-grid operator and the AF parameters would not permit a solution to be obtained for a highly oscillatory problem such as the previous sub-section's problem 3. Note that the equivalent smoothing rates on the present problems 2 and 3 are comparable to those for the previous problem 2.

Table V. Characteristics of the Rectangular Chebyshev-Fourier Test Problems

Problem No.	ε	m_u	m_a
1	0.00	1	1
2	0.10	1	1
3	0.20	2	2

Table VI. Parameters of the AF Scheme for the Rectangular Chebyshev-Fourier Problems

Level	α_ℓ	α_h	ω
2	0.5	6	1.0
3	2.0	75	1.0
4	10.0	1000	1.0
5	100.0	8000	1.0

Table VII. Equivalent Smoothing Rates on the Rectangular Chebyshev-Fourier Problems

Problem No.	AF/B	AF/D
1	.77	.75
2	.78	.79
3	.82	.76

Annular Chebyshev-Fourier Problem

The differential equation for this last linear example is

$$\frac{\partial}{\partial r}\left[r\, a\, \frac{\partial u}{\partial r}\right] + \frac{\partial}{\partial \theta}\left[\frac{1}{r}\, a\, \frac{\partial u}{\partial \theta}\right] = f \tag{61}$$

on $(1,5) \times (0,2\pi)$ with

$$a(r,\theta) = 1 + \varepsilon\, e^{\cos(m_a(r+\theta))} \tag{62}$$

$$u(r,\theta) = \cos(m_u \pi r)\, \sin(m_u \pi \cos\theta + \pi/4). \tag{63}$$

The radial boundary conditions are Dirichlet at $r = 5$ but Neumann at $r = 1$. Periodicity in azimuth is enforced. Tables VIII and IX present the test case and AF parameters, respectively.

The results are available in Table X. These are the least impressive smoothing rates of the linear test problems. Neumann boundary conditions are usually more troublesome than Dirichlet ones. The global approximation underlying the spectral methods makes them especially difficult to enforce.

Table VIII. Characteristics of the Annular Chebyshev-Fourier Test Problems

Problem No.	α	m_u	m_a
1	0.00	1	1
2	0.10	1	1
3	0.20	2	2

Table IX. Parameters of the AF Scheme for the Annular Chebyshev-Fourier Problems

Level	α_ℓ	α_h	ω
2	5	40	2.0
3	10	600	1.4
4	100	6000	1.0
5	1000	10000	1.0

Table 2. Equivalent Smoothing Rates on the Annular Chebyshev-Fourier Problems

Problem No.	AF/B	AF/D
1	.82	.87
2	.81	.87
3	.87	.86

VI. Potential Flow Past an Airfoil

The problem considered is that of compressible potential flow past a two-dimensional airfoil. We model this with the full potential equation, applying boundary conditions at the actual airfoil surface. In this work a numerically generated conformal mapping [23] is used to transform the airfoil onto the unit circle. The form of the transformation between the complex physical plane (the z-plane) and the complex computational plane (the σ-plane) is

$$\frac{dz}{d\sigma} = (1-\sigma)^{(1+\frac{\epsilon}{\pi})} e^{\sum_{n=1}^{N} (A_n+iB_n)\sigma^{(1-n)}}, \qquad (64)$$

where the coefficients A_n and B_n are generated numerically so that the known relations between the surface tangent angles and arc lengths of the airfoil shape are satisfied. The trailing edge of the airfoil is located at $\sigma = 1$ in the computational plane. The Schwarz-Christoffel factor in the transformation allows the smooth mapping of a finite-angle trailing edge. For further details on this particular mapping see Jameson [23]. The inner portion of a 16 × 48 grid is shown in Figure 1.

In the computational plane, with $\sigma = Re^{i\theta}$, the potential equation becomes

$$\frac{\partial}{\partial R}\left(R\rho \frac{\partial \Phi}{\partial R}\right) + \frac{\partial}{\partial \theta}\left(\frac{\rho}{R} \frac{\partial \Phi}{\partial \theta}\right) = 0, \tag{65}$$

where Φ is the velocity potential and ρ is the density, given by the isentropic relation

$$\rho = \left[1 - \frac{\gamma-1}{2} M_\infty^2 (q_r^2 + q_\theta^2 - 1)\right]^{\frac{1}{\gamma-1}}; \tag{66}$$

the ratio of specific heats is denoted by γ, the Mach number at infinity is denoted by M_∞, and the velocity components in the physical (r,θ) plane are

$$q_r = \frac{1}{H} \frac{\partial \Phi}{\partial R} \tag{67}$$

$$q_\theta = \frac{1}{RH} \frac{\partial \Phi}{\partial \theta}, \tag{68}$$

with

$$H = \left|\frac{dz}{d\sigma}\right|. \tag{69}$$

The boundary conditions at the surface and in the farfield are

$$\frac{\partial \Phi}{\partial R} = 0 \qquad \text{at} \quad R = 1 \tag{70}$$

$$\Phi \to R \cos \theta + E \tan^{-1}\left[\sqrt{1 - M_\infty^2} \tan \theta\right] \quad \text{as} \quad R \to \infty. \tag{71}$$

The first term in the farfield boundary condition describes the uniform freestream flow. The remaining term is the first-order lifting term; it is derived in [24]. The quantity E is known as the circulation. It is

determined by the Kutta condition, which states that the physical velocity at the trailing edge must be finite. Since $H = 0$ at the trailing edge, the Kutta condition reduces to

$$\frac{\partial \Phi}{\partial \Theta} = 0 \qquad \text{at} \quad \sigma = 1. \tag{72}$$

The singularity of the potential in the farfield poses difficulties (especially for spectral methods) that are best handled by computing in terms of the reduced potential G, which is defined by

$$G = \Phi - (R + \frac{1}{R}) \cos \Theta - E \tan^{-1}[\sqrt{1 - M_\infty^2} \tan \Theta] \tag{73}$$

and is assumed to be periodic in Θ. It follows that G satisfies

$$\frac{\partial}{\partial R}(R\rho \frac{\partial G}{\partial R}) + \frac{\partial}{\partial \Theta}(\frac{\rho}{R} \frac{\partial G}{\partial \Theta}) = 0, \tag{74}$$

along with

$$\frac{\partial G}{\partial R} = 0 \qquad \text{at} \quad R = 1 \tag{75}$$

$$G \to 0 \qquad \text{as} \quad R \to \infty, \tag{76}$$

and the Kutta condition.

The spectral method employs a Fourier series representation in Θ. Constant grid spacing in Θ corresponds to a convenient dense spacing in the physical plane at the leading and trailing edges. The domain in R (with a large, but finite outer cutoff) is mapped onto the standard Chebyshev domain $[-1,1]$ by an analytical stretching transformation that clusters the collocation points near the airfoil surface. The stretching is so severe that

the ratio of the largest-to-smallest radial intervals is over 1000 for the grid whose inner portion is illustrated in Figure 1. The transformation is incorporated into the operator which represents differentiation in the R direction.

Despite its nonlinearity the potential flow problem remains fairly straightforward so long as the flow is everywhere subsonic. The real difficulty of the problem arises when the flow forms a supersonic bubble on the airfoil. The potential equation is then of mixed elliptic-hyperbolic type and admits weak solutions with discontinuities. Both compression and expansion shocks will appear unless an artificial viscosity with a directional bias is introduced into the equation in the supersonic region. The most expedient technique for dealing with this is to use the artificial density approach of Hafez, et al. [25]. The original artificial density is

$$\tilde{\rho} = \rho - \mu \overset{+}{\delta} \rho \tag{77}$$

with

$$\mu = \max\left\{0, 1 - \frac{1}{M^2}\right\}, \tag{78}$$

where M is the local Mach number and $\overset{+}{\delta}\rho$ is an upwind first-order (undivided) difference. In the present work a higher-order artificial density formula related to a form developed by Jameson [13] has been employed.

The first pseudospectral solutions to the compressible potential flow problem were obtained by Streett [15], [26] using a single-grid version of the approximate factorization iterative scheme described in the fourth section. For subcritical flows this method was already highly competitive with state-of-the-art finite difference methods. For supercritical flows, however, the single-grid pseudospectral scheme was quite inefficient, even with the use of

the AF2 extension of the approximate factorization scheme. This problem, then, poses a useful application of the spectral multigrid approach and, as the results indicate, a dramatic demonstration of its effectiveness.

VII. Results for Potential Flow Past an Airfoil

The numerical examples of this section have been chosen primarily to illustrate the effectiveness of the multigrid approximate factorization (MG/AF) solution scheme in comparison with the earlier single-grid approximate factorization (SG/AF) method [15] for solving the spectral equations for potential flow. A secondary issue is the comparative quality of this spectral discretization and of widely-used finite difference approximations. A by-product of these examples is some practical guidelines for the multigrid algorithms.

Three test problems suffice for a comprehensive treatment of the spectral multigrid efficiency and spectral discretization accuracy issues: a subcritical lifting airfoil, a supercritical nonlifting airfoil, and a supercritical lifting airfoil. These have been listed in order of increasing difficulty. Detailed comparison of the spectral SG/AF and MG/AF schemes will be provided for the first two examples. Extensive comparisons are also made for all three problems between the spectral MG/AF scheme and two popular finite difference codes: TAIR [7], a single-grid/AF2 method and FLO36 [13], a multigrid/AF method.

Some of the relevant issues have already been discussed in [15]. The most sensitive matter is surely the weighing of the efficiency of two schemes (spectral and finite difference) with different accuracy and convergence properties. The reader is directed to [15] for a more detailed discussion than is provided here.

Three different grids have been used (with the coarser levels in parentheses): 16 × 32 (12 × 16 and 8 × 8), 16 × 48 (14 × 32, 12 × 16 and 8 × 8) and 18 × 64 (16 × 48, 14 × 32, 12 × 16 and 8 × 8). Note that in passing to a coarser level the grid is typically reduced by less than a factor of 2 in each coordinate direction. This choice leads to a significant improvement over the standard gridding for the spectral potential flow problem, especially in the supercritical regime where the solution has large high-frequency content.

This problem has the added complication of a highly-stretched grid in the radial direction. This is accounted for by changing the spectral differentiation matrices from $C^{-1}DC$ (see Eq. (2)) to

$$D = BC^{-1}DC, \tag{79}$$

where B is a diagonal matrix which contains the Jacobian of the transformation. A substantial improvement in the spectral multigrid algorithm results from defining the coarse-grid differentiation matrices directly by Eq. (39) rather than by the coarse-grid version of Eq. (79). In the absence of stretching these two definitions are equivalent. Equation (39) is easily and efficiently implemented with matrix-multiply techniques.

Virtually all the spectral multigrid results included here were obtained with the same fixed schedule: start on the finest grid, work down to the coarsest grid and then back up to the finest grid; on the way down there is 1 sweep though the (three) parameter sequence and on the way up there are 2 sweeps.

Subcritical Lifting Airfoil

The flow past an NACA 0012 airfoil at 4^{0} angle of attack and a freestream Mach number of 0.5 will serve as the first test case. The airfoil produces a fairly large lift coefficient at these conditions and the surface pressure distribution shows a sharp suction peak near the leading edge. Since the local Mach number in this peak is nearly 1, compressibility effects are substantial.

In order to demonstrate that the spectral solution on a relatively coarse grid captures all the essential details of the flow we first compare it with an extremely accurate finite difference result. In Figure 2 is shown the surface pressure coefficient from a spectral solution using 16 points in the radial (R) direction, and 32 points in the azimuthal (θ) direction; the symbols denote the solution at the collocation points. For comparison, the result from the finite difference code FL036 is shown as a solid line. The grid used in the benchmark finite difference calculation is so fine (64 × 384 points) that the truncation error is well below plotting accuracy. The spectral calculation seems to lack detail near the leading edge suction peak. However, since the spectral solution is actually a continuous representation of the solution, it may be expanded in terms of its basis functions onto a much finer mesh. Such an expansion, shown in Figure 3, reveals the hidden detail of the solution. The FL036 and expanded spectral results are identical to plotting accuracy. The spectral computation on this mesh yields a lift coefficient with truncation error less than 10^{-4}. Spectral solutions on a 16 × 32 grid are thus of more than adequate resolution and accuracy for subcritical flows.

The convergence histories for both the SG/AF and the MG/AF spectral schemes on this test case are displayed in Figures 4 and 5. The convergence

histories have been supplied for both the maximum residual (Figure 4) and the error in circulation (Figure 5). They are plotted against machine time on a CDC Cyber-175 computer. Although the multigrid code (henceforth referred to as "MGAFSP") shows a substantial improvement over the single-grid approximate factorization code ("AFSP") in maximum residual convergence, the gain is even more dramatic from the lift convergence standpoint. This is understandable since the lift is predominantly a low-frequency property of the solution. The single-grid spectral approximate factorization scheme was recognized to be weak in damping for long-wavelength error components [15].

The consensus in the computational transonics community appears to be that TAIR is the fastest widely-available finite difference code. A comparison of maximum residual versus machine time for TAIR and MGAFSP on the subcritical test case is shown in Figure 6. The two codes require nearly equivalent machine time with TAIR showing a better asymptotic convergence rate. However, the TAIR result was produced on a rather coarse (default) finite difference mesh of 30 × 149 points. Compared with the surface pressure results from MGAFSP and FL036, the TAIR result is significantly in error near the leading edge (Figure 7). This is indeed truncation error, because TAIR results on a 60 × 297 mesh are more in agreement with those of MGAFSP and FL036. A further indication of the somewhat large truncation error of the TAIR result is that the predicted drag and lift coefficients are correct to only two decimal places (subcritical potential flow yields identically zero drag).

In Figure 8 are shown convergence histories from TAIR, FL036, and MGAFSP on meshes which yield approximately equivalent accuracy; the surface pressure results are the same to plotting accuracy, the lift coefficient is converged in the third decimal place, and the predicted drag coefficient is less than

.001. (Actually, the spectral result is an order of magnitude more accurate than these limits, but the TAIR result barely meets them.) As can be seen from Figure 4, the single-grid AFSP result would fall in the vicinity of the FLO36 and TAIR results in the present figure.

Use of more than three grids in the spectral multigrid code did not yield an improvement in effective convergence, since the interpolation overhead became a greater proportion of the total work. It would have been desirable to use a lowest grid coarser than 8×8 in the multigrid cycle. Unfortunately, due to the presence of the metric singularity at the trailing edge, coarser mesh results were so oscillatory as to provide no useful long-wavelength information.

Supercritical Nonlifting Airfoil

The test is again the NACA 0012 but at $M_\infty = 0.8$ and with zero angle of attack, i.e., a nonlifting condition. The surface pressure coefficient distribution as computed by the spectral method on an 18×64 grid is displayed in Figure 9. The shock at mid-chord is relatively strong; the normal Mach number ahead of the shock is approximately 1.25. The shock is spread over several mesh spaces by the finite difference artificial viscosity used in the spectral calculation. Although this shock is already far sharper than those produced by finite difference codes on a comparable grid, it ought to be possible to capture the shock in a still smaller region with a spectral method employing an artificial viscosity more suited to the spectral discretization.

The convergence histories for the SG/AF scheme (combining AF2 and AF1) and the MG/AF scheme (using AF1 alone) on a fine grid are shown in Figure 10. The multigrid scheme obviously shows a much higher asymptotic convergence

rate. Note that the single-grid scheme initially oscillates with the maximum residual of order unity for a rather lengthy period. This is indicative of the lack of high-frequency damping in the AF2 scheme. The flowfield is being established in this period by the AF2 scheme; the plot of the history of the number of supersonic points in Figure 11 shows that the AF2 scheme establishes the shock position and the size of supersonic region nearly as fast as the multigrid scheme, albeit with some transient overshoot. This rapid establishment of the flowfield is at the expense of high-frequency error, which is subsequently damped when the AF2/AF1 alternate cycling is begun. The multigrid algorithm, however, monotonically establishes the flowfield and damps high-frequency errors in a far more efficient manner.

Experience with all forms of transonic potential flow calculations has shown that convergence rates are quite sensitive to the order and amount of artificial viscosity: more artificial viscosity generally yields faster convergence, but at the expense of more widely smeared shocks. Multigrid schemes have been especially sensitive to these effects, and the present one is no exception. However, the large improvement in efficiency offered by the multigrid over the previous single-grid spectral scheme has allowed the use of much finer grids, offsetting the present, uncomfortably large artificial viscosity.

Supercritical Lifting Airfoil

The lifting supercritical test case was the NACA 0012 at $M_\infty = 0.75$ and $\alpha = 2^\circ$, which yields a section lift coefficient of nearly 0.6. A shock appears only on the upper surface for these conditions and is rather strong for a potential calculation; the normal Mach number ahead of the shock is about 1.36. Lifting supercritical test cases are especially difficult for

spectral methods since the solution will always have significant content in the entire frequency spectrum; the shock populates the highest frequencies of the grid and the lift is predominantly on the scale of the entire domain. An iterative scheme therefore must be able to damp error components across the spectrum. The AF2/AF1 scheme of [15] was somewhat unreliable for such problems; so a comparison will not be shown between AF2/AF1 and the multigrid scheme.

A history of the surface pressure coefficient is supplied in Figure 12. This demonstrates the rapid convergence of the entire frequency spectrum of the solution. Pressure distributions are shown after 0, 1, 4, and 9 cycles of the fixed-cycle algorithm; one cycle requires approximately 5 seconds of Cyber-175 time. The shock overshoot seen in the 4-cycle frame is a phenomenon associated with the final positioning of the shock by the multigrid scheme. The finite difference multigrid scheme exhibits similar behavior [13].

All of the supercritical spectral multigrid calculations shown thus far used a sequence of five rather than three grids, mostly due to the finer finest grid used for these cases. Scheduling within the fixed-cycle multigrid algorithm was much the same as for the subcritical cases: one or two passes through the time-step sequence were made on each grid. Convergence for supercritical cases is not always monotonic because adjustments in lift or shock position can introduce high-frequency errors which may require an extra cycle to damp. An adaptive cycle algorithm might be of benefit here provided that the "limit cycle" problem were avoided.

Surface pressure distributions, both at the collocation points and spectrally expanded onto finer spacing, are shown in Figures 13 and 14 for grids of 16 × 48 and 18 × 64 points, respectively. As can be seen, the coarser-grid result predicts virtually the same shock position as the finer-

grid computation; the lift coefficients agree to 1%. These results may be compared with those from the finite difference codes, TAIR and FL036, shown in Figures 15 and 16, respectively. The shock predicted by TAIR is far more rounded and smeared than that of FL036, reflecting the coarser mesh and larger artificial viscosity used in the former. The TAIR result shown is also only correct to one decimal place in lift as compared with a finer-grid result. Convergence histories for these four cases: spectral multigrid (16 × 48) and (18 × 64), TAIR (30 × 149), and FL036 (32 × 192) are shown in Figure 17. The spectral results are obviously handicapped in this comparison by the necessity of such fine (for spectral methods) meshes brought about by the use of the finite difference artificial viscosity form. Perhaps the purely spectral shock-capturing methods currently under development will permit sharp shocks to be captured with still coarser meshes.

VIII. Conclusions

Spectral multigrid methods are still in their infancy. Nevertheless, they have already exhibited the capacity to accelerate drastically iterative schemes for nonlinear, as well as linear, problems. Rough estimates of the asymptotic convergence rates indicate that the multigrid procedure has led to an improvement over the single-grid spectral method of nearly a factor of 10 for subcritical cases; the improvement is considerably greater for supercritical situations.

The worth of the spectral discretization itself for compressible flows is now clear: equivalent solutions are indeed obtained with far fewer grid points than are required for finite difference solutions. Since subcritical flows are smooth, the present results, showing both that the spectral method

convergence rate is far better than second-order and also that its absolute error level is lower than finite difference ones even on unreasonably coarse grids, are no surprise. Undeniably, any shock discontinuity in supercritical flow should produce some degradation in the formal accuracy of the spectral solution. Nonetheless, grid refinement studies demonstrate that the spectral solutions stabilize on far coarser grids than do finite difference solutions. Coupled with multigrid solution techniques, spectral methods for steady compressible flows have reached the stage at which they are truly competitive with finite difference methods on problems of aerodynamic interest.

Several aspects of this technique have to be improved before spectral methods for compressible flows reach their full maturity. The present relaxation schemes are just straightforward modifications of the ones used for finite difference methods. Surely relaxation schemes more tuned to the spectral discretization can and will be devised. There is also the clear need to develop more suitable forms of artificial viscosity for capturing shocks by spectral methods.

References

[1] Streett, C. L.: "Viscous-Inviscid Interaction for Transonic Wing-Body Configurations Including Wake Effects." AIAA Journal, Vol. 20, pp. 915-923, 1982.

[2] Murman, E. M. and Cole, J. D.: "Calculation of Plane Steady Transonic Flow, AIAA Journal, Vol. 9, pp. 114-121, 1971.

[3] Ballhaus, W. F.: "Some Recent Progress in Transonic Flow Computations," Numerical Methods in Fluid Dynamics, Wirz, H. and Smolderen, J. J., eds., McGraw Hill, 1977.

[4] Jameson, A.: "Transonic Flow Calculations," Numerical Methods in Fluid Dynamics, Wirz, H. and Smolderen, J. J., eds., McGraw Hill, 1977.

[5] Ballhaus, W. F., Jameson, A., and Albert, J.: "Implicit Approximate Factorization Schemes for the Efficient Solution of Steady Transonic Flow Problems," AIAA Journal, Vol. 16, pp. 573-579, 1978.

[6] Holst, T. L.: "Implicit Algorithm for the Conservative Transonic Full-Potential Equation Using an Arbitrary Mesh," AIAA Journal, Vol. 17, pp. 1038-1045, 1978.

[7] Holst, T. L.: "A Fast, Conservative Algorithm for Solving the Transonic Full-Potential Equation," AIAA Paper 79-1456, 1979.

[8] Baker, T. J.: "A Fast Implicit Algorithm for the Nonconservative Potential Equation," Open Forum Presentation at the AIAA 4th Computational Fluid Dynamics Conference, Williamsburg, VA, July 1979.

[9] Catherall, D.: "Optimum Approximate Factorization Schemes for Two Dimensional Steady Potential Flows," AIAA Journal, Vol. 20, pp. 1057-1063, 1982.

[10] Wong, Y. S. and Hafez, M.: "Conjugate Gradient Methods Applied to Transonic Finite Difference and Finite Element Calculations," AIAA Journal, Vol. 20, pp. 1526-1533, 1982.

[11] Doria, M. L. and South, J. C.: "Transonic Potential Flow and Coordinate Generation for Bodies in a Wind Tunnel," AIAA Paper 82-0223, 1982.

[12] South, J. C. and Brandt, A.: "The Multi-Grid Method: Fast Relaxation for Transonic Flows," Advances in Engineering Science, NASA CP-2001, Vol. 4, pp. 1359-1369, 1976.

[13] Jameson, A., "Acceleration of Transonic Potential Flow Calculations on Arbitrary Meshes by the Multiple Grid Method," AIAA Paper 79-1458, 1979.

[14] Hussaini, M. Y., Kopriva, D. A., Salas, M. D., and Zang, T. A.: "Spectral Methods for Euler Equations," presented at the AIAA 6th Computational Fluid Dynamics Conference, Danvers, MA, July 1983.

[15] Streett, C. L.: "A Spectral Method for the Solution of Transonic Potential Flow About an Arbitrary Airfoil," presented at the AIAA 6th Computational Fluid Dynamics Conference, Danvers, MA, July 1983.

[16] Zang, T. A., Wong, Y. S., and Hussaini, M. Y.: "Spectral Multigrid Methods for Elliptic Equations," Journal of Computational Physics, Vol. 48, pp. 485-501, 1982.

[17] Zang, T. A., Wong, Y. S., and Hussaini, M. Y.: "Spectral Multigrid Methods for Elliptic Equations II," submitted.

[18] Brandt, A.: "Multi-level Adaptive Solution to Boundary Value Problems," Mathematics of Computation, Vol. 31, pp. 333-391, 1977.

[19] Hackbusch, W.: "On the Multi-Grid Method Applied to Difference Equations," Computing, Vol. 20, pp. 291-306, 1978.

[20] Nicolaides, R. A.: "On Multiple Grid and Related Techniques for Solving Discrete Elliptic Systems," Journal of Computational Physics, Vol. 19, pp. 418-431, 1975.

[21] Wesseling, P.: "Theoretical and Practical Aspects of a Multigrid Method," SIAM J. on Scientific and Statistical Computing, Vol. 3, pp. 387-407, 1982.

[22] Douglas, J. and Gunn, J. E.: "A General Formulation of Alternating Direction Method," Numerische Mathematik, Vol. 6, pp. 428-453, 1964.

[23] Jameson, A.: "Iterative Solution of Transonic Flows Over Airfoils and Wings, Including Flows at Mach 1," Communications on Pure and Applied Mathematics, Vol. 27, pp. 283-309, 1974.

[24] Ludford, G. S. S.: "The Behavior at Infinity of the Potential Function of a Two-Dimensional Subsonic Compressible Flow," Journal of Mathematical Physics, Vol. 30, pp. 117-130, 1951.

[25] Hafez, M. M., South, J. C., and Murman, E. M.: "Artificial Compressibility Methods for Numerical Solution of Transonic Full Potential Equation," AIAA Journal, Vol. 17, pp. 838-844, 1979.

[26] Gottlieb, D., Lustman, L., and Streett, C. L.: "Spectral Methods for Two-Dimensional Shocks," Proc. of the Symposium on Spectral Methods, SIAM CBMS Series, 1983.

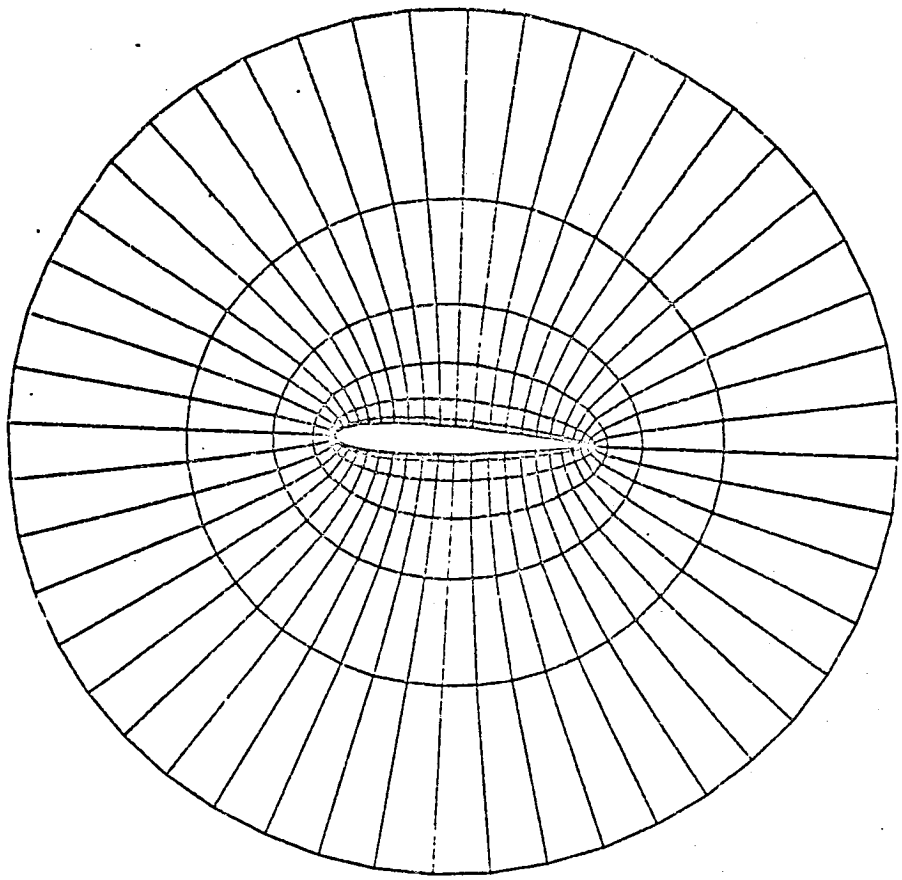

Figure 1. Grid about NACA 0012 airfoil

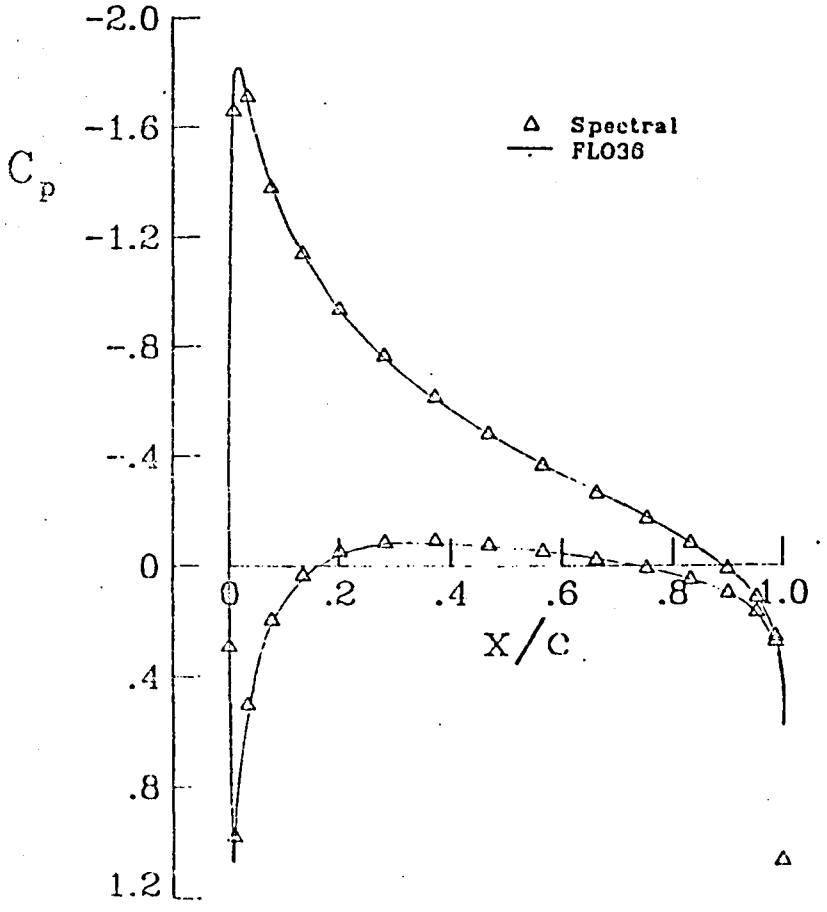

Figure 2. Comparison of surface pressure coefficient distributions
Spectral: 16 × 32 points
FKO36: 16 × 192 points
NACA 0012, M = 0.5, α = 4°

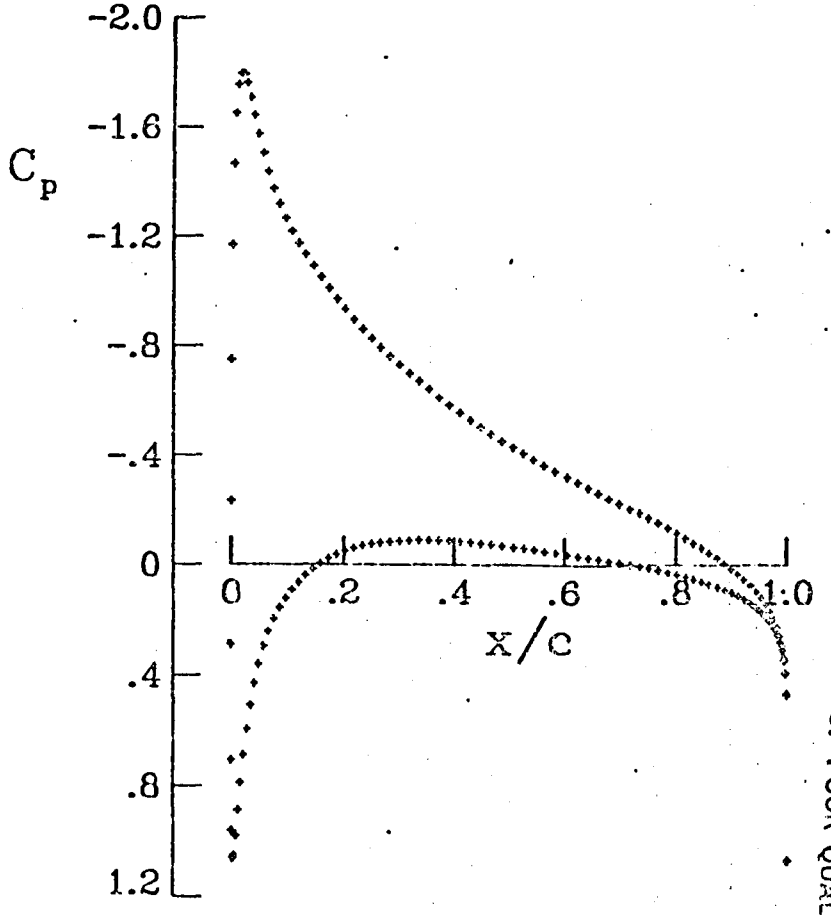

Figure 3. Surface pressure coefficient from expanded spectral solution
16 × 32 points
NACA 0012, M = 0.5, α = 4°

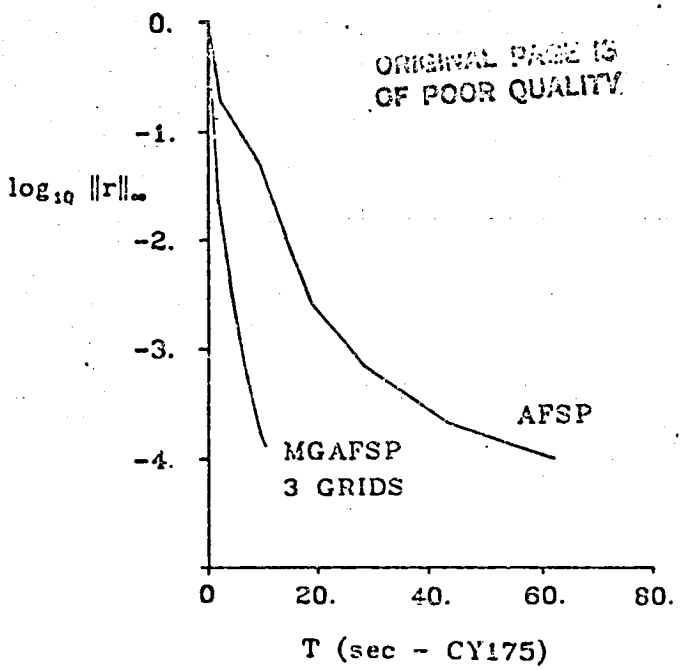

Figure 4. Maximum residual vs. machine time multigrid and single-grid schemes NACA 0012, $M = 0.5$, $\alpha = 4^o$

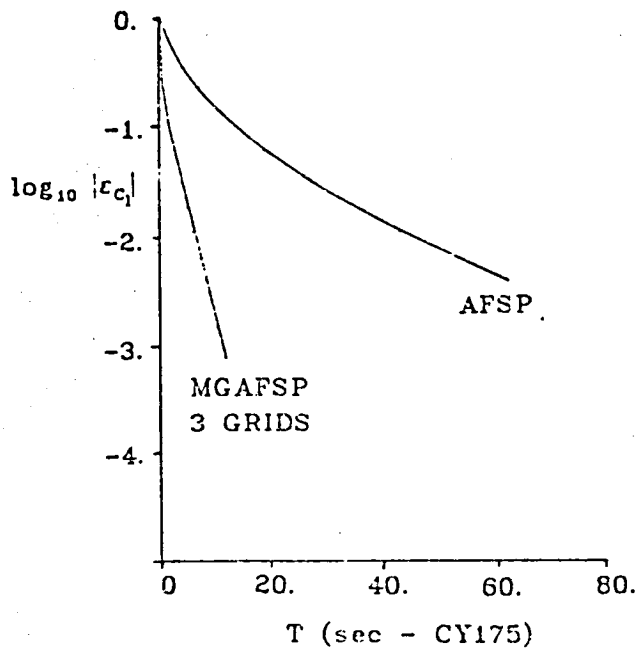

Figure 5. Error in lift vs. machine time multigrid and single-grid schemes NACA 0012, $M = 0.5$, $\alpha = 4^o$

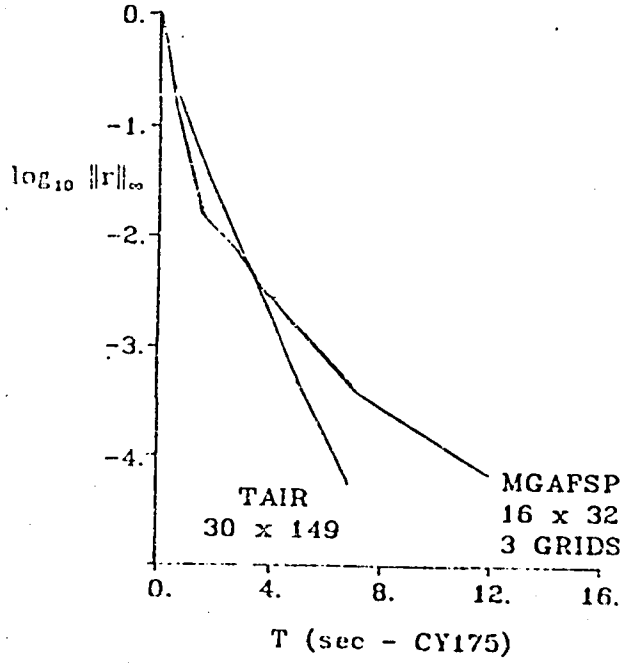

Figure 6. Maximum residual vs. machine time
NACA 0012, M = 0.5, $\alpha = 4^\circ$

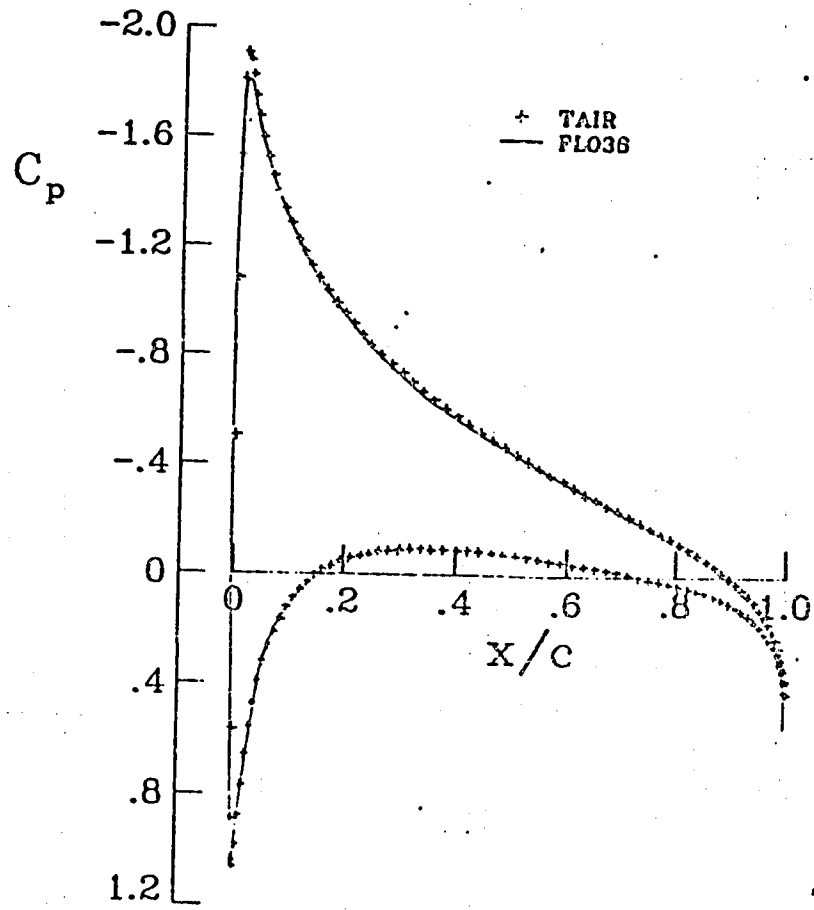

Figure 7. Comparison of surface pressure coefficient distributions
TAIR: 30 × 149 points
FL036: 32 × 192 points
NACA 0012, M = 0.5, $\alpha = 4^\circ$

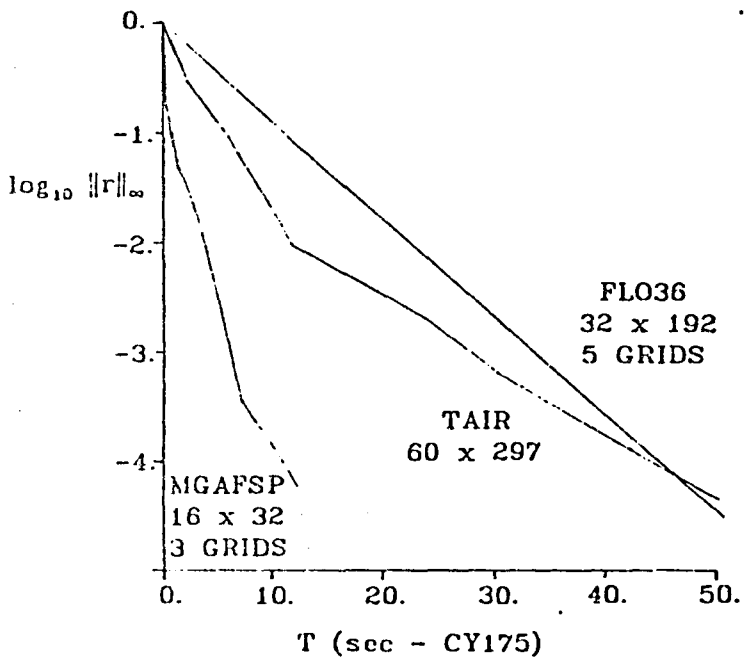

Figure 8. Maximum residual vs. machine time
NACA 0012, M = 0.5, $\alpha = 4^\circ$

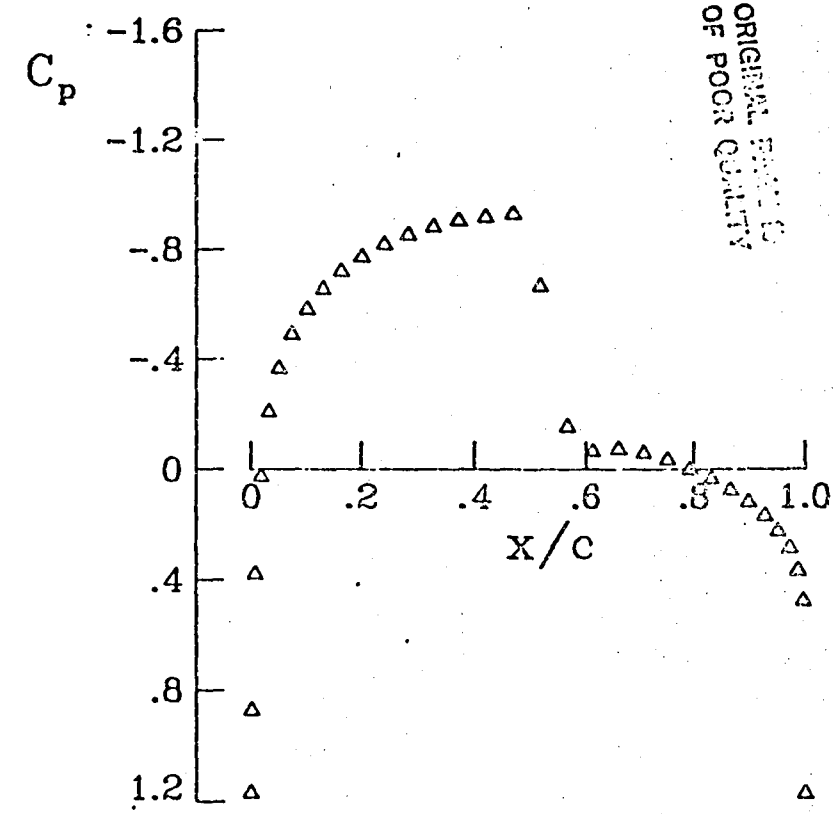

Figure 9. Surface pressure coefficient
spectral solution: 18 x 64 points
NACA 0012, M = 0.8, $\alpha = 0$

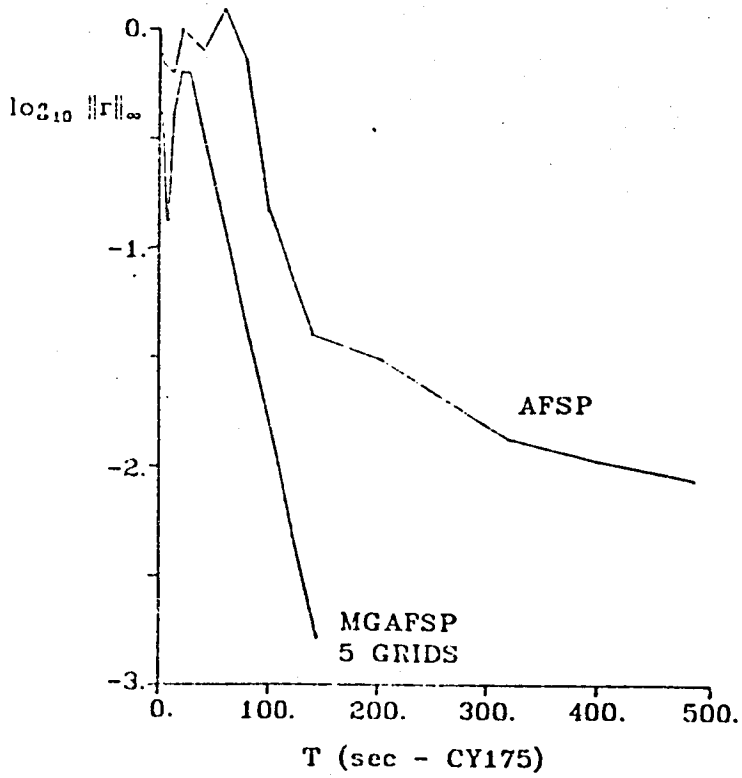

Figure 10. Maximum residual vs. machine time multigrid and single-grid schemes NACA 0012, M = 0.8, α = 0

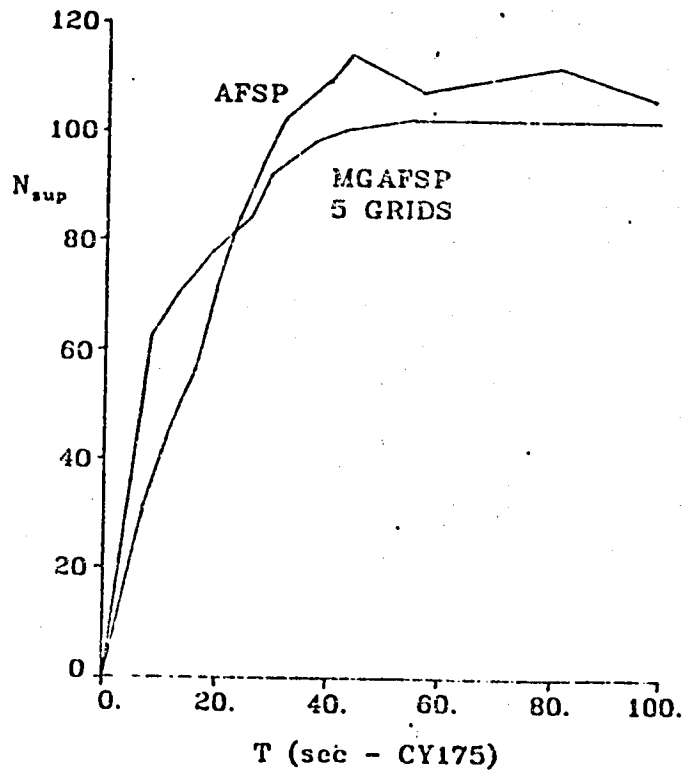

Figure 11. Number of supersonic points vs. machine time NACA 0012, M = 0.8, α = 0

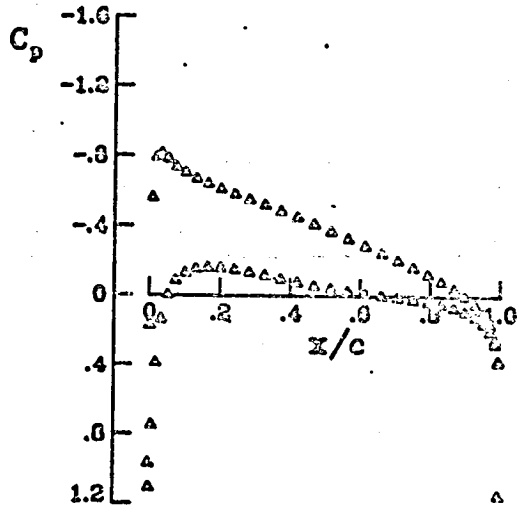

a. Initial condition

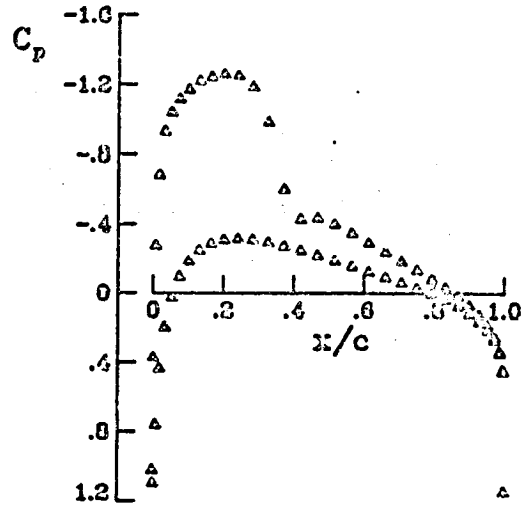

b. After 1 cycle

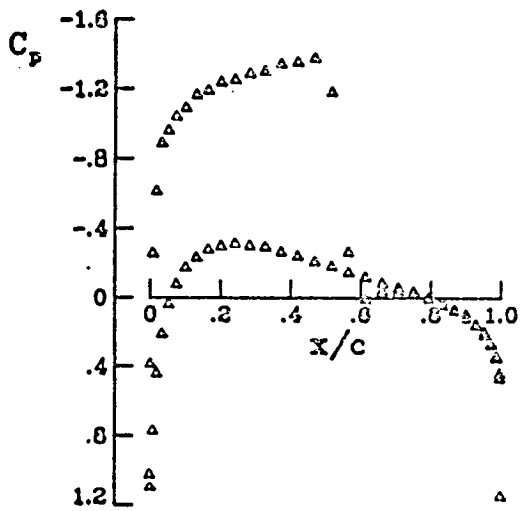

c. After 4 cycles

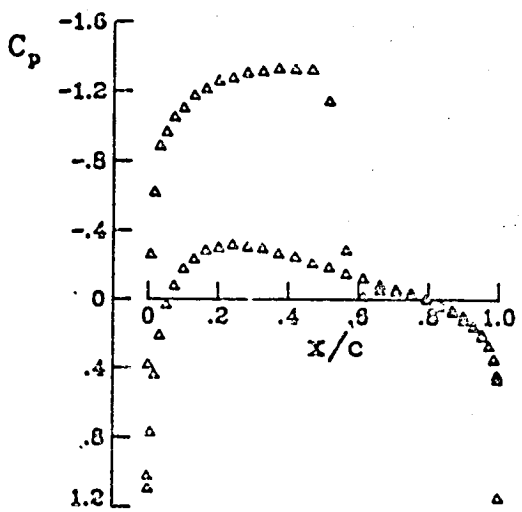

d. After 9 cycles

Figure 12. History of surface pressure coefficient distribution
spectral solution: 18 × 64 points
NACA 0012, $M = 0.75$, $\alpha = 2^{\circ}$

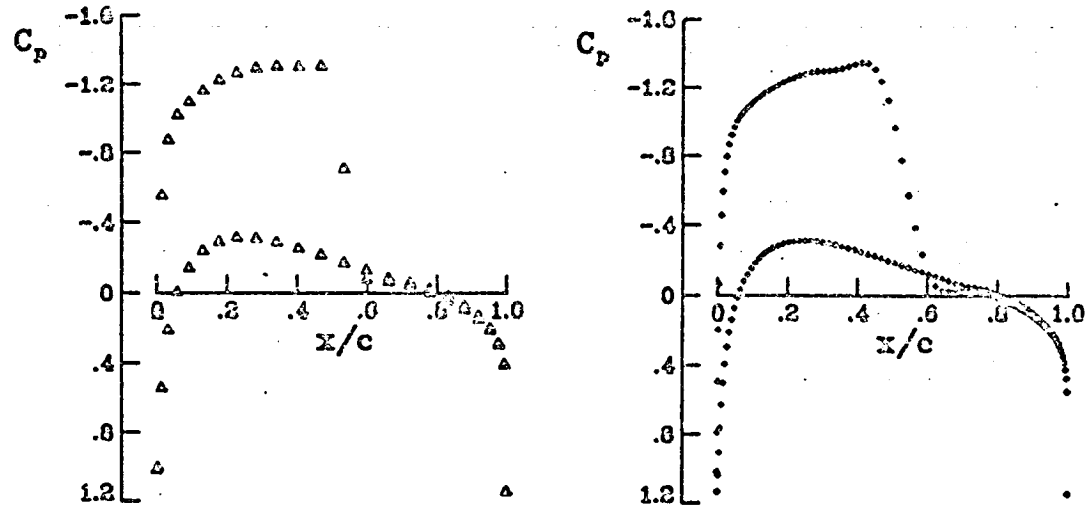

a. Collocation points b. Expanded

Figure 13. Surface pressure coefficient distribution spectral solution 16 × 48 points
NACA 0012, M = 0.75, $\alpha = 2^{\circ}$

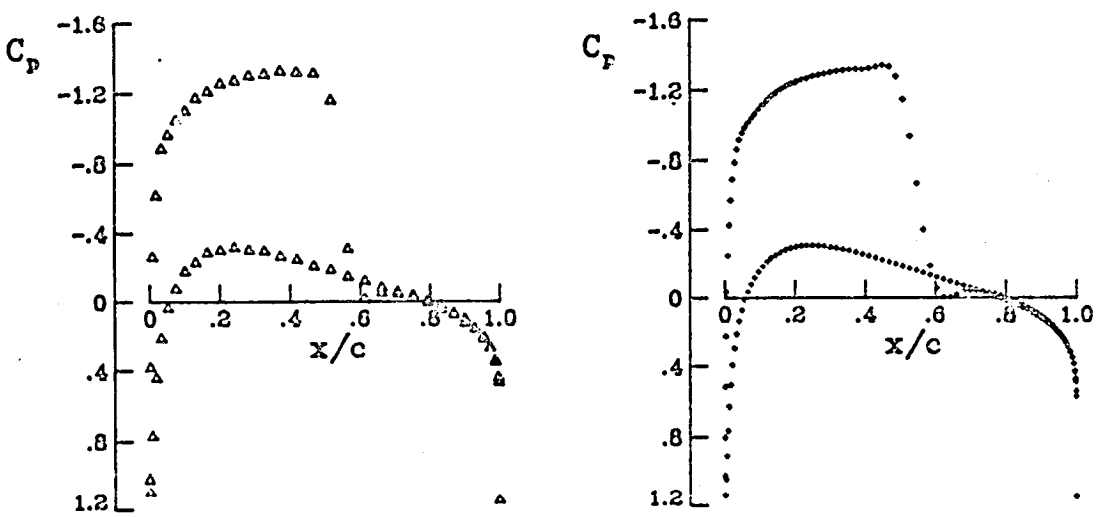

a. Collocation points b. Expanded

Figure 14. Surface pressure coefficient distribution spectral solution: 18 × 64 points
NACA 0012, M = 0.75, $\alpha = 2^{\circ}$

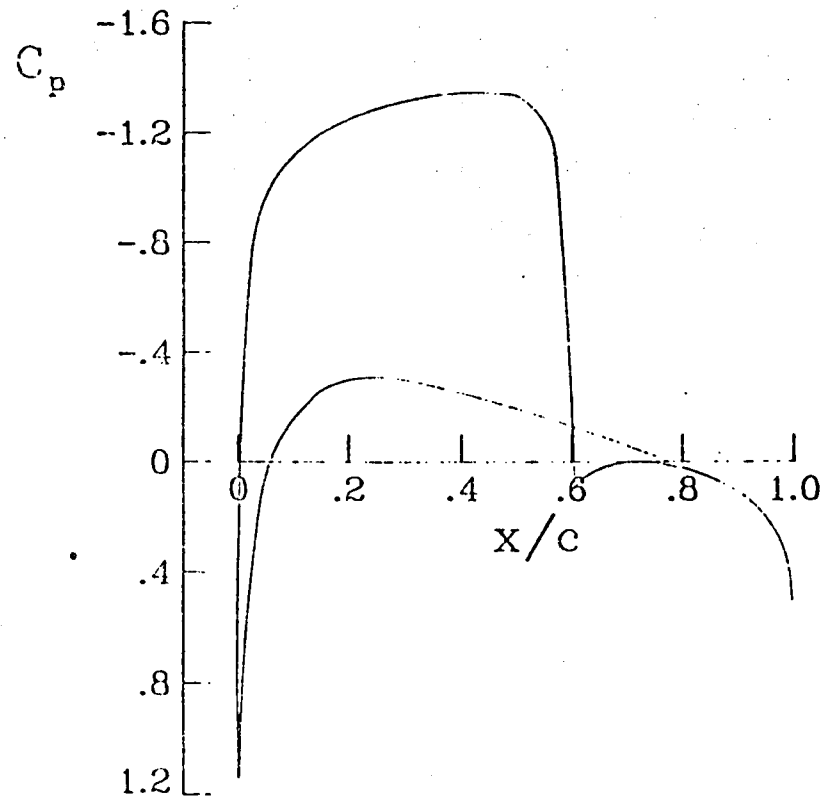

Figure 15. Surface pressure coefficient distribution
TAIR: 30 × 149 points
NACA 0012, M = 0.75, α = 2°

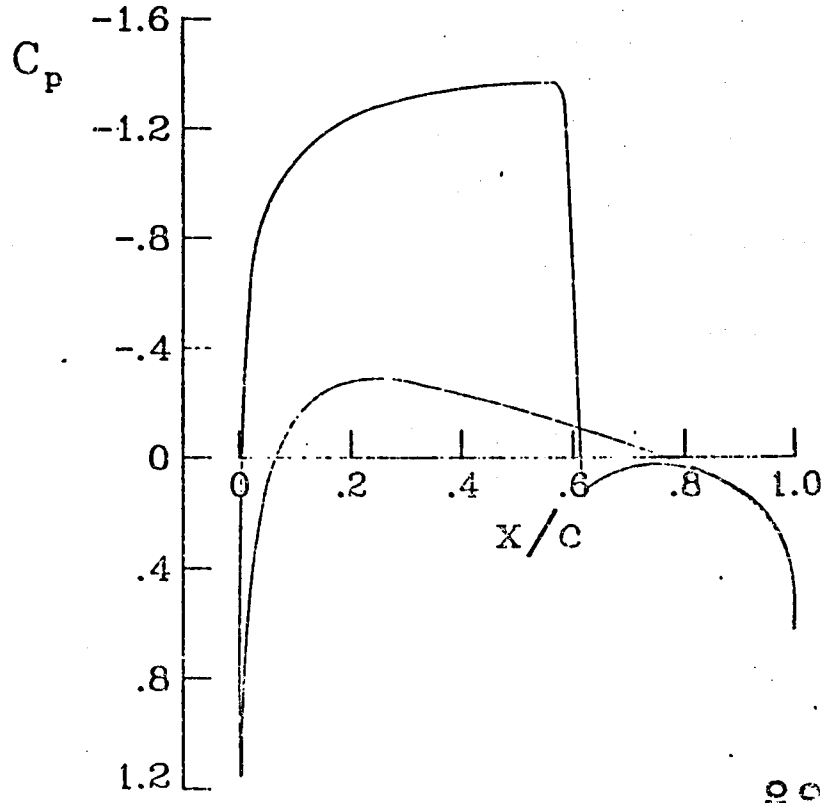

Figure 16. Surface pressure distribution
FLO36: 32 × 192 points
NACA 0012, M = 0.75, α = 2°

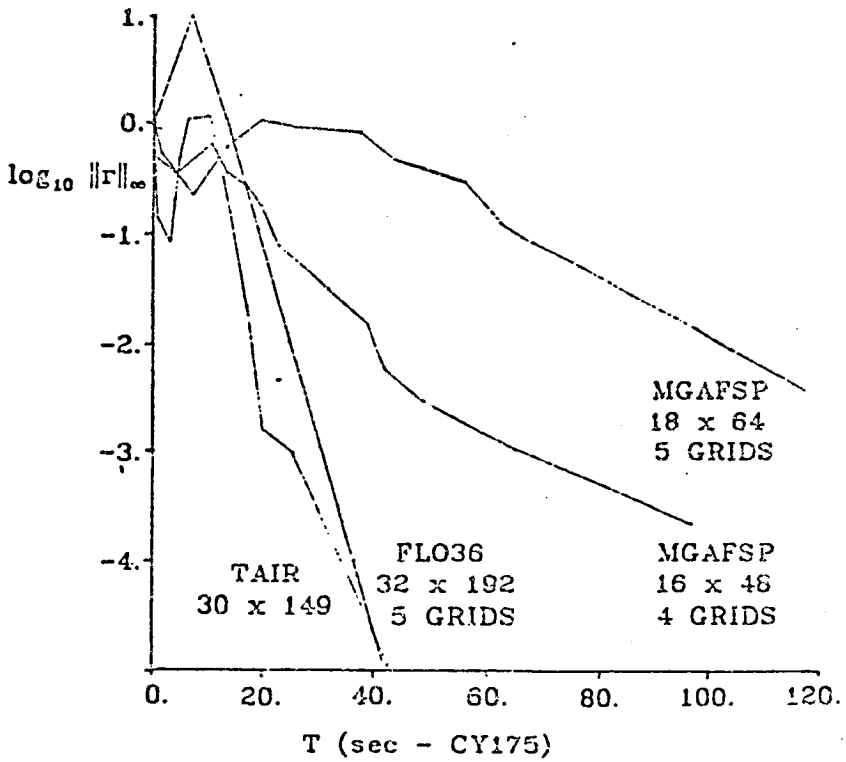

Figure 17. Maximum residual vs. machine time
NACA 0012, $M = 0.75$, $\alpha = 2^\circ$

END

DATE

FILMED

NOV 4 1983